The Enhanced Photocatalytic Activity of $Mn_xCo_{1-x}Fe_2O_4$ Over the $Zn_xCo_{1-x}Fe_2O_4$ Under the Visible Light Irradiation: A Comparative Study

M. SRINIVAS and L. GOMATHI DEVI[*]

Department of Post Graduate Studies in Chemistry, Central College City Campus,
Dr. Ambedkar Street, Bangalore University, Bangalore-560001, India
gomatidevi_naik@yahoo.co.in

Abstract: $Zn_xCo_{1-x}Fe_2O_4$ and $Mn_xCo_{1-x}Fe_2O_4$ (where x=0.5 atom %) catalysts were synthesized by sol-gel technique and were further characterized by various analytical techniques. PXRD pattern confirms cubic spinel structure for both the samples. UV-Visible spectra show extended absorption in the visible region and the band gap values of $Zn_{0.5}Co_{0.5}Fe_2O_4$ and $Mn_{0.5}Co_{0.5}Fe_2O_4$ catalysts were found to be 1.71 and 1.67 eV. Photocatalytic of experiments show that $Mn_{0.5}Co_{0.5}Fe_2O_4$ is a better photocatalyst compared to the $Zn_{0.5}Co_{0.5}Fe_2O_4$ due to the unique characteristics of Mn^{2+} ion which can exist in different oxidation states.

Keywords: Enhanced Photocatalytic Activity, Visible Light Irradiation, Metal oxides, Preparation of Metal complexes

Introduction

The ferrites are mixed metal oxides of considerable technological importance[1-5]. Ferrites have the general form of $M^{II}Fe_2^{III}O_4$ (AB_2O_4). Some ferrites adopt normal spinel structure and others adopt inverse spinel structure. The unit cell contains 32 oxygen atoms in a perfect cubic close packed array. In normal spinel structure 8 'A' metal atoms occupy tetrahedral sites and 16 'B' metal atoms occupy octahedral sites and the structure can be visualized as being built up of alternating cubelets of ZnS type and NaCl type structure. The two factors that determine which combination of atoms can form a spinel type structure are: a) total formal cation charge, and b) the relative sizes of two cations with respect to each other and with respect to the oxygen anions. The charge balance should be such a way that solid should be electrically neutral. Most of the A^{II} cations have radii in the range of 0.65-0.95 Å for six coordination and the radii of B^{III} should be predominantly in the range of 0.60-0.70 Å. The larger cations do not form oxide spinels. $CoFe_2O_4$ is mixed metal oxide with spinel structure. It is found to be stable in aqueous media. $CoFe_2O_4$ can act as a good absorber of visible light to initiate various redox reactions since it posse's suitable lower band gap[6-9]. The electronic properties of $CoFe_2O_4$ can be altered by the addition of dopant ions into the structure.

The dopant chosen in the present research work include Zn^{2+} and Mn^{2+} cations. The electronic configuration of Zn and Mn cations are [Ar] $3d^{10} 4s^2$ and [Ar] $3d^5 4s^2$ respectively. Mn posse's half filled d-orbital and Zn posses completely filled electronic state which is very stable. The ionic radius of Co^{2+}, Zn^{2+} and Mn^{2+} are 0.70, 0.74 and 0.80 Å respectively. The incorporation of these ions into $CoFe_2O_4$ at Co^{2+} lattice site is not expected to change the spinel structure. However, many of the oxides may not posses normal spinel structure. Several factors influence the structure. Whether a given spinel oxide will adopt normal or inverse spinel structure depends on factors which include: a) relative sizes of A and B, b) Madelung constant for the normal and inverse spinel structure, c) ligand field stabilization energies of cations on tetrahedral and octahedral sites and d) polarization and covalence effects. Normal spinel structure or inverse/ disordered spinel structure will be adopted by the metal oxide based on the above factors. The electrical and magnetic properties of spinel compounds depend on the composition of the ferrite, its use temperature and precise cation arrangement. An extensive study of these compounds in connection with solid state electronic industry is the need of the day. In the electronic industries if 'A' cation is replaced by either Mn or Zn, the material is referred to as soft ferrites which are generally used in sweep transformer and deflection yoke of a television set. Hence in the present research work, incorporation of Zn^{2+} and Mn^{2+} ions at Co^{2+} lattice site in the $CoFe_2O_4$ is attempted. $Zn_{0.5}Co_{0.5}Fe_2O_4$ and $Mn_{0.5}Co_{0.5}Fe_2O_4$ were synthesized by sol-gel combustion method. The concentration of Mn and Zn was optimised to 0.5 atom % such that the native $CoFe_2O_4$ structure is not disrupted and at the same time the incorporated ions should suitably replace the host Co^{2+} ions. This replacement is possible since the ionic radii of Mn^{2+} and Zn^{2+} ions suitably match with the ionic radius of 'A' cation (Co^{2+}). If the concentration of the dopant ions is increased above 0.5 atom %, formation of new compounds of the type $MnFe_2O_4$ and $ZnFe_2O_4$ takes place. The incorporation of these dopant ions into the host $CoFe_2O_4$ structure leads to the creation of dopant energy levels below the conduction band edge and these energy levels may facilitate efficient charge transfer process in a photochemical reaction. An attempt is made to study the opto-electronic properties of $Zn_{0.5}Co_{0.5}Fe_2O_4$ and $Mn_{0.5}Co_{0.5}Fe_2O_4$ catalysts in comparison with $CoFe_2O_4$. Their use as a photocatalyst in energy and environment applications is attempted.

Experimental

Acid orange (AOII) was obtained from sigma Aldrich. Citric Acid (CA), cobalt nitrate ($Co(NO_3)_2.6H_2O$), zinc nitrate ($Zn(NO_3)_2.6H_2O$), manganese nitrate ($Mn(NO_3)_2.6H_2O$) and iron nitrate ($Fe(NO_3)_2.6H_2O$) were obtained from Sisco-chemical industries. All chemicals were analytical grade reagents and were used without further prification. Double distilled water was used in all the experiments.

Preparation of $CoFe_2O_4$ and $Zn_{0.5}/Mn_{0.5}Co_{0.5}Fe_2O_4$ samples

The adopted procedure for the preparation of Zn and Mn doped $CoFe_2O_4$ was similar to the method adopted by James wang et al.,[10].

The citric acid (CA) is used as chelating agent and a solution of it was prepared by dissolving 5% w/v and the solution was heated at 70 ^{0}C to obtain clear solution. To the above clear solution, stoichiometric amounts (0.5/0.5:2 ratio). $Co(NO_3)_2.6H_2O$, $Fe(NO_3)_3.9H_2O$ and $Zn(NO_3)_26H_2O$/ $Mn(NO_3)_26H_2O$ were added in accordance with the stoichiometric molecular formula $Mn_{0.5}Co_{0.5}Fe_2O_4$ and $Zn_{0.5}Co_{0.5}Fe_2O_4$. The solution was evaporated by stirring and heating for 4 hours at 70 °C until it turns into a solid gel. Finally, the product was calcined in a furnace for 2 hours at 800 °C. $Co(NO_3)_2.6H_2O$ and $Fe (NO_3)_3.9H_2O$ were taken in the ratio of 1:2 for the preparation of $CoFe_2O_4$ and similar procedure was adopted.

Characterization techniques

The catalysts were characterized by the following techniques: powder X-ray diffraction (PXRD), UV-Vis absorption spectroscopic technique, X-ray energy dispersive spectroscopy (XEDS) and photoluminescence (PL) spectroscopy. The details of instrumentation and photocatalytic degradation experiments are given in the literature[11].

Results and Discussion

PXRD

The PXRD pattern of $CoFe_2O_4$, $Zn_{0.5}Co_{0.5}Fe_2O_4$ and $Mn_{0.5}Co_{0.5}Fe_2O_4$ catalysts are shown in the Figure 1. The pattern of the prepared $CoFe_2O_4$ and the doped samples can be indexed to the pure cubic phase and it matches with the standard pattern of $CoFe_2O_4$ (JCPDS No 22-1086). The 2θ values along with the respective hkl values can be indexed as $18.21^0(111)$, 30.15^0 (220), 35.40^0 (311), 36.97^0 (222) 43.12^0 (400), 53.46^0 (422), 56.97^0 (511), 62.58^0 (440), $71.36(622)$ and 72.96^0 (533). The crystallite size was calculated by using the Scherrer's equation: $D = K \lambda / \beta \cos \theta$, where, λ is the wavelength, β is full width at half maximum diffraction plane, k is a shape factor and θ is angle of diffraction. The crystallite sizes of $CoFe_2O_4$, $Zn_xCo_{1-x}Fe_2O_4$ and $Mn_xCo_{1-x}Fe_2O_4$ were found to be 50.52, 27.83 and 14.64 nm respectively. The ionic radius of Mn^{2+} (0.80 Å) is greater than Co^{2+} (0.70 Å). Therefore, Mn^{2+} ions cannot act as interstitial impurity in the $CoFe_2O_4$ matrix. Hence Mn^{2+} ions can possibly act as substitutional impurity at the lattice sites of Co^{2+}. The higher ionic radius of Mn^{2+} ion produces a localized perturbation in the $CoFe_2O_4$ lattice due to its slight increase in the ionic size. The crystallite size decreases with incorporation of Mn^{2+} ions due to the inhibition effect on grain growth which favours the increase in the total grain boundary energy. The decrease in the crystallite size of Mn^{2+} doped sample may lead to the increase in the specific surface area. This would also increase the density of surface state defects on the surface of $CoFe_2O_4$ grains. $Mn_{0.5}Co_{0.5}Fe_2O_4$ sample with smaller crystallite size would contain a large number of lattice defects.
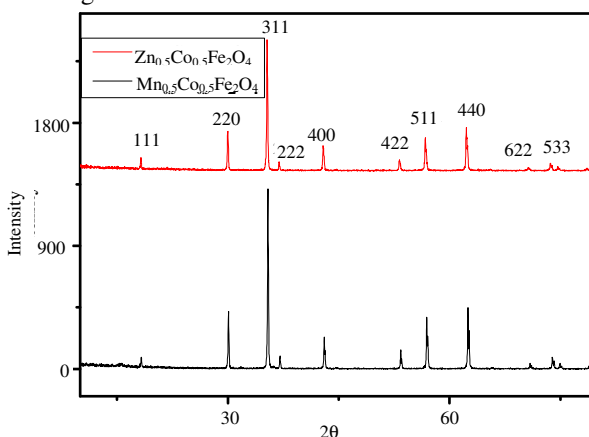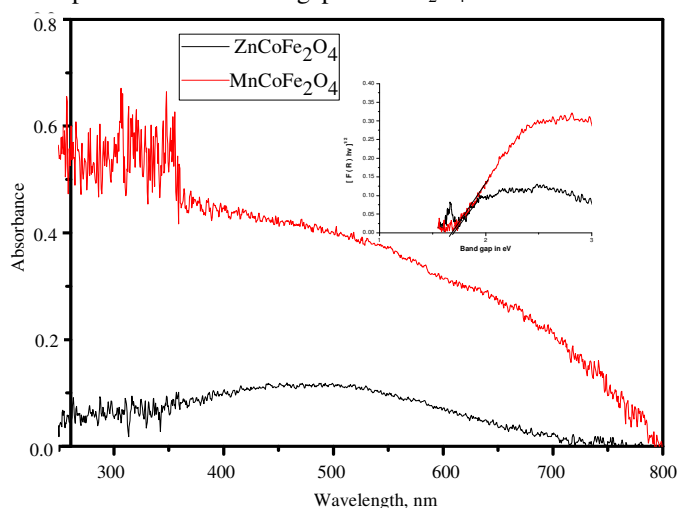

Figure 1. PXRD pattern of $Zn_{0.5}Co_{0.5}Fe_2O_4$ and $Mn_{0.5}Co_{0.5}Fe_2O_4$ catalysts

UV-Visible absorbance spectroscopy

UV-visible absorption spectra of $CoFe_2O_4$, $Zn_{0.5}Co_{0.5}Fe_2O_4$ and $Mn_{0.5}Co_{0.5}Fe_2O_4$ catalysts are shown in the Figure 2. Continuous absorption is observed from 300-700 nm for all the samples.

$Mn_{0.5}Co_{0.5}Fe_2O_4$ sample shows extended absorption up to 800 nm and the extent of absorption is also higher for $Mn_{0.5}Co_{0.5}Fe_2O_4$ sample compared to $Zn_{0.5}Co_{0.5}Fe_2O_4$ and $CoFe_2O_4$. Fe^{III} like Mn^{II} has d^5 electronic configuration and its absorption spectrum might therefore be expected to consist of similarities of weak spin-forbidden band. However, a crucial difference between these ions is that Fe^{III} carries an additional positive charge and posse's greater ability to polarize and hence produces intense charge transfer absorption at much lower energies than Mn^{II} ions. Charge transfer band extends up to visible region due to the weak d-d band transitions. Full analysis of d-d spectrum of Fe^{III} / Mn^{II} / Co^{II} is rather difficult and the spectrum shows continuous absorption. The UV-visible absorption spectra and Kubelka-Munk plot of $CoFe_2O_4$ is represented in our previous study[12]. The band gap values of $CoFe_2O_4$, $Zn_{0.5}Co_{0.5}Fe_2O_4$ and $Mn_{0.5}Co_{0.5}Fe_2O_4$ were calculated by using Kubelka-Munk plot and the values were found to be 2.73, 1.71 and 1.67 eV respectively as shown in the inset of Figure 2. The band gap values of the doped samples decreases due to the presence of dopant energy levels and also due to the defect energy levels created by the incorporation of dopant within the band gap of $CoFe_2O_4$.

**Figure 2.** UV-visible absorbance spectra of $Zn_{0.5}Co_{0.5}Fe_2O_4$ and $Mn_{0.5}Co_{0.5}Fe_2O_4$ catalysts. Kubelka-Munk plot is shown in the inset

XEDS analysis

XEDS patterns of $Zn_{0.5}Co_{0.5}Fe_2O_4$ and $Mn_{0.5}Co_{0.5}Fe_2O_4$ samples are given in Figure 3. XEDS pattern of $CoFe_2O_4$ is given elsewhere[12]. This technique confirms the presence of Zn / Mn, Co, Fe and O atoms and their proportions in the prepared samples. Incorporation of Mn^{2+} ions into the $CoFe_2O_4$ lattice was energetically more efficient compared to the incorporation of Zn^{2+} ions. The atomic percentages of all the ions are given in Table 1.

Table 1. Elemental composition of $Zn_{0.5}Co_{0.5}Fe_2O_4$ and $Mn_{0.5}Co_{0.5}Fe_2O_4$ samples by XEDS

Element	Weight %	Atomic %	Element	Weight %	Atomic %
O	23.89	53.25	O	11.48	31.25
Fe	45.34	28.96	Mn	24.58	19.49
Co	16.63	10.06	Fe	49.59	38.66
Zn	14.14	7.72	Co	14.35	10.60
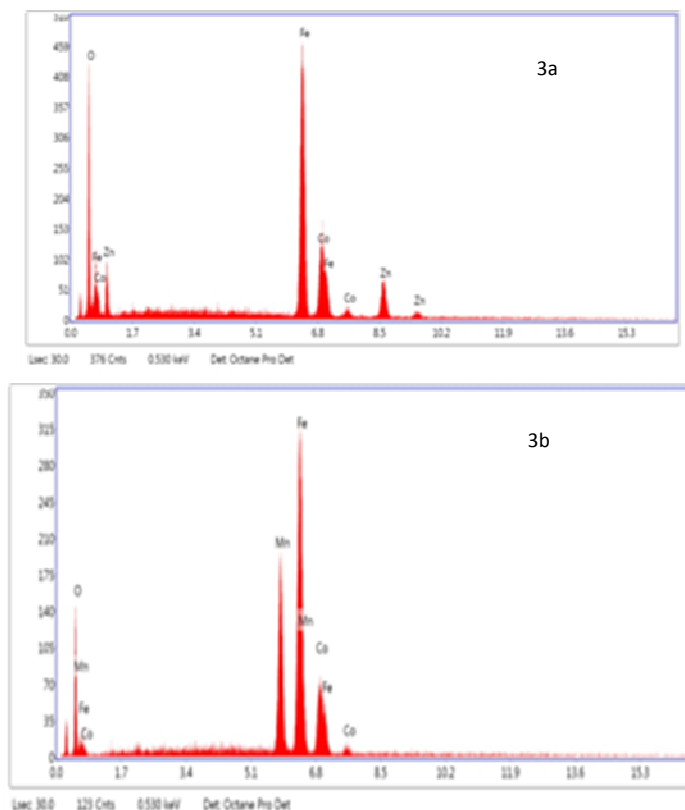
Figure 3. XEDS micrographs of (a) $Zn_{0.5}Co_{0.5}Fe_2O_4$ and (b) $Mn_{0.5}Co_{0.5}Fe_2O_4$ catalysts

*Photoluminescence (PL) Spectra*

The fundamental information regarding the energy levels lying within the band gap states can be obtained from the PL technique. The PL emission is obtained as a result of recombination of excited electron-hole pair. Lower PL intensity indicates efficiency charge carrier separation. Three bands are observed at 439 nm (2.82 eV), 482 nm (2.57 eV) and 542 nm (2.28 eV) as shown in the Figure 4. The observed band at 439 nm is due to the electronic transitions taking place between the valence band and conduction bands. The bands observed in the visible region can be due to either the d-d transitions and also due to the transitions taking place invariably involving defect states created in the lattice. It was observed that the PL spectra of $Mn_{0.5}Co_{0.5}Fe_2O_4$ sample shows lower intensity compared to the PL spectrum of $CoFe_2O_4$ implying lower extent of recombination of photogenerated charge carriers. The intensity has decreased by 61%. The PL intensity of $Zn_{0.5}Co_{0.5}Fe_2O_4$ has decreased by 41% compared to $CoFe_2O_4$. Dopant energy levels in the $Mn_{0.5}Co_{0.5}Fe_2O_4$ sample facilitates the charge transfer process, may be due to the presence of Mn^{2+} ions which can show multiple oxidation states. The dopant energy levels may act as a shallow trap for the charge carriers. These charge carriers can be detrapped easily to the energetically favourable other states. This process reduces the recombination of photogenerated charge carriers. In the case of $Zn_{0.5}Co_{0.5}Fe_2O_4$ sample, Zn can only show an oxidation state of +2. Hence, certain extent of recombination may take place in this sample.
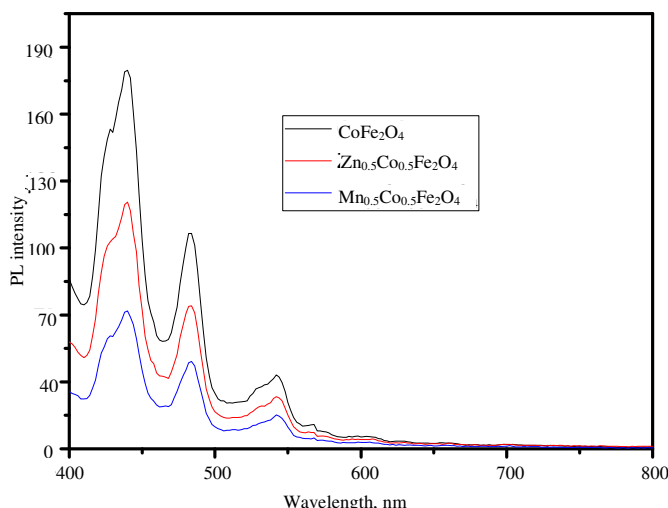
Figure 4. PL spectra of $CoFe_2O_4$, $Zn_{0.5}Co_{0.5}Fe_2O_4$ and $Mn_{0.5}Co_{0.5}Fe_2O_4$ catalysts

Photocatalytic activity

The photocatalytic degradation of AOII in presence of $CoFe_2O_4$, $Zn_{0.5}Co_{0.5}Fe_2O_4$ and $Mn_{0.5}Co_{0.5}Fe_2O_4$ catalysts was studied under the illumination of visible light and the time taken for the degradation is found to be 300, 250 min and 200 min respectively (Figure 5). The plot of C/C_o versus time is shown in the Figure 5, where C_o and C are the concentration of AOII substrate molecule at time 0 and time t respectively. The degradation data was analysed for pseudo first order kinetic model which generally suits for heterogeneous photocatalytic degradation reactions, since the initial concentration of AOII substrate molecule is low. The rate law can be stated as: $\log (C/C_o) = -kt$ where, k is pseudo first order rate constant. By plotting $\log C/C_o$ as a function of irradiation time, the rate constant can be calculated from the slopes of simulated straight lines. Table 2 shows the rate constant values, duration of degradation and percentage degradation values. It is observed that photocatalytic efficiency of $Mn_{0.5}Co_{0.5}Fe_2O_4$ is 63% higher than the $CoFe_2O_4$. The efficiency of $Zn_{0.5}Co_{0.5}Fe_2O_4$ is 48% higher than the $CoFe_2O_4$. The higher photocatalytic activity of $Mn_xCo_{1-x}Fe_2O_4$ can be accounted in the following way: a) smaller crystallite size of the sample as observed from the PXRD pattern, b) higher extent of absorption as observed from the UV-visible absorption spectrum, c) lower PL intensity showing lesser recombination of photogenerated charge carriers, d) its unique half filled electronic configuration facilitates the trapping of photogenerated electrons and these trapped electrons gets detrapped to the adsorbed oxygen molecule or to the intermediate organic radicals generated in the degradation reactions. This trapping and detrapping process is very efficient in this catalyst to maintain the stable half filled electronic configuration. This process reduces the recombination of photogenerated charge carriers to major extent and increases the efficiency of the degradation process, e) Mn is capable of showing multiple oxidation states during the reaction process, f) efficient migration of charge carriers at the interface leading the generation of higher concentration of active free radicals, g) interfacial charge transfer process (IFCT) increases as the excited electrons can also reduce Fe^{3+} to Fe^{2+} ions. These Fe^{2+} ions intern gets reoxidised to Fe^{3+} state through the multi electron reduction of oxygen, and h) the Fe^{3+} ions at the surface can serve as oxygen reduction site.
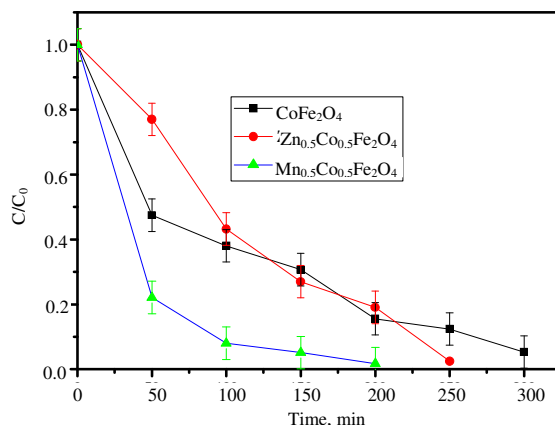
Figure 5. Plot of C/C_o *vs*. time in minutes for the degradation of AOII (10 ppm) in presence of $CoFe_2O_4$, $Zn_{0.5}Co_{0.5}Fe_2O_4$ and $Mn_{0.5}Co_{0.5}Fe_2O_4$ catalysts

The photocatalytic activity of $Zn_{0.5}Co_{0.5}Fe_2O_4$ is intermediate between $Mn_{0.5}Co_{0.5}Fe_2O_4$ and $CoFe_2O_4$. The band gap of this catalyst is found to be 1.71 eV and PL spectra shows higher recombination compared to the $Mn_{0.5}Co_{0.5}Fe_2O_4$ catalyst. Zn doesn't show multiple oxidation states like Mn. It can only show +2 oxidation state by losing 4s electrons. The $3d^{10}$ energy levels are found to be more stable and is not expected to show multiple oxidation states. The activity of $Zn_{0.5}Co_{0.5}Fe_2O_4$ catalyst also depends on the pH conditions of the reactions. The catalyst is found to be stable only in the acidic pH and known to get corroded at higher pH values as per literature[13].

Table 2. Rate constant, degradation time and percentage degradation values for the degradation of AOII using $CoFe_2O_4$, $Zn_{0.5}Co_{0.5}Fe_2O_4$ and $Mn_{0.5}Co_{0.5}Fe_2O_4$ catalysts

Catalysts	Rate constant $x10^{-2}$ min^{-1}	Degradation time, min	% Degradation
$CoFe_2O_4$	0.55	300	96
$Zn_{0.5}Co_{0.5}Fe_2O_4$	1.04	250	97
$Mn_{0.5}Co_{0.5}Fe_2O_4$	1.5	200	99

Conclusion

$Zn_{0.5}Co_{0.5}Fe_2O_4$ and $Mn_{0.5}Co_{0.5}Fe_2O_4$ catalysts were synthesized by sol-gel combustion method. PXRD pattern confirms cubic spinel structure for both the doped catalysts. The PL spectra show lesser recombination of photogenerated charge carriers for $Mn_{0.5}Co_{0.5}Fe_2O_4$ catalyst compared to $Zn_{0.5}Co_{0.5}Fe_2O_4$ catalyst. The photocatalytic activity of $Mn_{0.5}Co_{0.5}Fe_2O_4$ catalyst is higher than the activity of $CoFe_2O_4$ and $Zn_{0.5}Co_{0.5}Fe_2O_4$ due to multiple beneficial characteristics of doped Mn ions.

References

1. Borgarello E, Kiwi J, Gratzel M, Pelizzetti E and Visca M, *J Am Chem Soc.,* 1982, **104(11)**, 2996-3002; DOI:10.1021/ja00375a010

2.   Yamashita H, Ichihashi Y, Takeuchi M, Kishiguchi S and Anpo M, J *Synchrotron Radiat.,* 1999, 6, 451-452: DOI:10.1107/S0909049598017257
3.   Takeuchi M and Anpo M, *Int J Photoenergy*, 2001, **3(2),** 89-94; DOI:10.1155/S1110662X01000101
4.   Valenzuela M A, Bosch P, Jimenez-Becerrill J, Quiroz O and Paez A I, *J Photochem Photobiol A*, 2002, **148(1-3),** 177-182; DOI:10.1016/S1010-6030(02)00040-0
5.   Borse P H, Jang J S, Hong S J, Lee J. S, Jung J H, Hong T E, Jeong E D, Hong K S, Yoon J H and Kim H G, *J Korean Phys Soc.,* 2009, **55(4),** 1472-1477; DOI:10.3938/jkps.55.1472
6.   Yang H, Lu J Z, Cheng X and Tang Y, *J Alloys Compds.*, 2009, **476(1)** 715-719; DOI:10.1039/x0xx00000x
7.   Huheey E, Keiter E A and Keiter R L, *Pearson Education Singapore*, 4th Ed., 2006.
8.   Matzapetakis M, Karligiano N, Bino A, Dakanali M, Raptopoulou P, Angoulis V, Terzis A,Giapintzakis J and Salifoglou, *Inorg Chem.,* 2000, 39 (23) 4044−4051; DOI:10.1021/ic010276n
9.   Dom R, Subasri R, Radha K and Borse H, *Solid State Commun.,* 2011, **151(6),** 470-473; DOI:10.1016/j.ssc.2010.12.034
10.   Noppakun S, Christopher C, Berndt, Cuie W and James W, *Acta Biomaterialia* 2013**, 9(3),** 5830-5837; DOI:10.1016/j.actbio.2012.10.037
11.   Gomathi Devi L and Srinivas M, *J Environ Chem Eng.,* 2017, 5, 3243-3255; DOI:10.1016/j.jece.2017.06.023
12.   Srinivas M and Gomathi Devi L, *Int J Res Eng Technol.,* 2018, 2319-2321; 10.15623/ijret.2018.0709004
13.   Engenidou E, Fytianos K and Poulios I, *App Cat B: Environ.*, 2005, **59,** 81-89; DOI:10.1016/j.apcatb.2005.01.005